

THE CATASTROPHIC FRAGMENTATION OF COMET P/2010 V1 (IKEYA-MURAKAMI)

KLEyna, J. T.¹, YE, Q.-Z.², HUI, M.-T.³,
MEECH, K. J.¹, WAINSCOAT, R.¹, MICHELI, M.^{1,4,5,6}, KEANE, J. V.¹, WEAVER, H. A.⁷¹Institute for Astronomy, University of Hawai'i at Manoa, Honolulu, HI, 96822, USA; kleyna@ifa.hawaii.edu²Department of Physics and Astronomy, The University of Western Ontario, London, Ontario N6A 3K7, Canada³Earth, Planetary, and Space Sciences, UCLA, Los Angeles, CA 90095⁴SSA NEO Coordination Centre, European Space Agency, 00044 Frascati (RM), Italy⁵Istituto di Astrofisica e Planetologia Spaziali, Istituto Nazionale di Astrofisica, 00133 Roma (RM), Italy⁶SpaceDyS s.r.l., 56023 Cascina (PI), Italy and⁷The Johns Hopkins University Applied Physics Laboratory, Laurel, Maryland, 20723, USA

ABSTRACT

We describe 2016 January and February observations of the fragments of P/2010 V1, a comet previously observed in a 2010 October outburst (Ishiguro et al. 2014). We present photometry of the fragments, and perform simulations to infer the time of breakup. We find that the eastern-most rapidly brightening fragment (*F4*) best corresponds to the original nucleus, rather than the initial bright fragment *F1*. We compute a radial non-gravitational force A_1 consistent with zero, and a non-zero tangential component $A_2 = (+7.93 \pm 2.26) \times 10^{-9}$ AU day⁻². Monte Carlo simulations indicate that the fragments were emitted on the outbound journey well after the 2010 outburst, with bright fragment *F1* splitting in mid-2013 and the fainter fragments within months of the 2016 January recovery. Western fragment *F7* is the oldest, dating from 2011. We suggest that the delayed onset of the splitting is consistent with a self-propagating crystallization of water ice.

Keywords: comets: individual (P/2010 V1)

1. INTRODUCTION

A comet discovered in PanSTARRS1 (Kaiser et al. 2002) survey data on 2015 Dec. 31 (Weryk et al. 2016) was determined to be the recovery of comet P/2010 V1 (Ikeya-Murakami), which was discovered in 2010 after a massive outburst (Ishiguro et al. 2014). Follow up observations using MegaCam on the Canada-France-Hawai'i telescope (CFHT) on 2016 January 1 showed another comet $\sim 100''$ southeast of P/2010 V1. Subsequent observations showed the new comet had many pieces and was undergoing a fragmentation. Sekanina (2016a) suggested that the breakup began in 2010 and that what appeared to be the most eastern-most nucleus (our *F2*) is the primary; Dekelver & Cuppens (2016) subsequently argued that a new further-east component (their *C*, our *F4*¹ is the primary.

We obtained data on 12 nights between 1 January and 10 February 2016, and identified at least 17 fragments, some of which are shown in Fig. 1). The situation is very dynamic with rapid changes in brightness between fragments and new components appearing (fragment *F9* appeared on January 7). Both the initial outburst and this splitting event are observed near perihelion (True Anomaly $TA = 11^\circ$ in 2010; $-44^\circ < TA < -21^\circ$ here.)

Comet splitting may be common, but detailed characterization of a split nucleus is relatively rare. There have been observations of ~ 45 split comets in the last 150 years, with only a handful well studied (Boehnhardt 2004). Splitting is an efficient mass loss mechanism for comets, and is important in their evolution. Two types of splitting are known: (1) splitting into a few (~ 2) pieces, and (2) splitting into many sub-km fragments. Various

mechanisms – e.g., tides, rotation, thermal stress, gas pressure, and impacts – have been proposed for splitting (Boehnhardt 2004), but only in the case of Shoemaker-Levy 9 was the mechanism well understood (tidal breakup, Sekanina et al. (1994)). Importantly, the size distribution and composition the ejected material can be related to the internal structure of the comet (Belton 2015).

In this paper, we present photometry and astrometry of the fragments of P/2010 V1, and perform dynamical simulations to examine the time span over which P/2010 V1 broke up. We attempt to use the time of the breakup in relation to perihelion to infer the breakup mechanism.

2. OBSERVATIONS

Our principal observations were obtained with MegaCam on the 3.6m CFHT telescope, on 2006 1 January to 10 February (Table 1). The two initial nights used the *r* filter with exposures of 60s and 90s. Subsequent nights were observed in the more sensitive wide-band *gri* filter for 120s to 180s. Additionally, we obtained *R*-band observations with the UH2.2m and Tek2048, on UT 16 Jan 2015 in the middle of the gap between CFHT runs.

Conditions were good on all nights, with little variation in the photometric zero point, and seeing FWHM ranged from $0.7''$ to $1.7''$.

Figure 1 shows the rapid evolution of the sub-nuclei in relative and absolute brightness, position, and distinctness.

We found additional *i* and *r*-band images in the PanSTARRS1 (PS1) archive from 2015 Oct 10 and 2015 December 4. No evidence of any fragments is seen in October, but fragment *F1* and the *F2* through *F6* cluster are seen in December. Because these are short 45s images on a small 1.8m telescope, it was necessary to stack four

¹ Fig. 2 contains a translation of IAU fragment designations to our *F_n* identifiers.

Table 1
Observations

UT Date	UT Times	Telescope/Instrument	Filter	FWHM ^a	No. exp. ^b	Exp. time ^c	r_h ^d	Δ ^e	α ^f	TA ^g
2016-01-01	11:36–11:40	CFHT/MegaCam	<i>r</i>	0.78	3	60	1.73	0.82	18.68	-43.35
2016-01-02	11:30–11:35	CFHT/MegaCam	<i>r</i>	0.74	3	90	1.72	0.82	18.34	-42.84
2016-01-03	13:39–13:44	CFHT/MegaCam	<i>gri</i>	0.69	3	120	1.72	0.81	17.96	-42.29
2016-01-05	13:00–13:16	CFHT/MegaCam	<i>gri</i>	1.12	5	180	1.71	0.79	17.27	-41.28
2016-01-06	12:50–13:09	CFHT/MegaCam	<i>gri</i>	0.75	6	180	1.71	0.79	16.92	-40.76
2016-01-07	13:38–13:46	CFHT/MegaCam	<i>gri</i>	0.90	3	180	1.71	0.78	16.56	-40.23
2016-01-08	10:06–13:14	CFHT/MegaCam	<i>gri</i>	0.91	12	180	1.70	0.77	16.24	-39.75
2016-01-16	08:53–12:01	UH2.2m/Tek2048	<i>open</i>	0.93	5	600	1.68	0.73	13.58	-35.55
2016-01-30	09:27–09:35	CFHT/MegaCam	<i>gri</i>	1.53	3	180	1.64	0.67	11.43	-27.85
2016-01-31	11:47–11:55	CFHT/MegaCam	<i>gri</i>	1.50	3	180	1.63	0.67	11.50	-27.23
2016-02-05	09:58–10:06	CFHT/MegaCam	<i>gri</i>	1.51	3	180	1.62	0.66	12.33	-24.43
2016-02-10	10:15–10:23	CFHT/MegaCam	<i>gri</i>	1.72	3	180	1.61	0.65	13.86	-21.53

^a Median point source FWHM in arcsec.

^b Number of exposures.

^c Exposure time, in seconds.

^d Heliocentric distance, AU.

^e Geocentric distance, AU.

^f Phase angle, degrees.

^g True anomaly, degrees.

images to see the December PS1 *r*-band detections.

3. PHOTOMETRY

The MegaCam images were bias-subtracted and flattened by the Elixir pipeline at CFHT. We fit a world coordinate system (WCS) using the AstrOmatic SWARP tool (Bertin et al. 2002), and used our custom calibration pipeline to give an absolute magnitude calibration using SDSS DR8 (Aihara et al. 2011). For the *r* filter, we ignored the minor 1% difference between SDSS *r* and MegaCam *r*. For the broadband *gri* filter, we used a transformation to a *gri* AB magnitude computed by Simon Prunet (personal communication), where

$$gri_{AB} = -2.5 \log_{10}[0.4388 \times 10^{-0.4g} + 0.4146 \times 10^{-0.4r} + 0.1490 \times 10^{-0.4i}] \quad (1)$$

and *g*, *r* and *i* are SDSS AB magnitudes. Using measurements of fragments *F1* and *F4* in a pair of images on 30 Jan, we convert *r* to *gri* as $gri = r + 0.18$, and present all photometry.

Because the fragments were crowded, diffuse, and (for *F2* and *F3*) overlapping, we applied a simple aperture correction to compute individual magnitudes. We computed the magnitude of isolated fragment *F1* in each image in a large 5'' diameter aperture, and used this to correct the magnitude of all measured fragments to a smaller 2'' aperture. Additionally, we increased the size of this calibration aperture inversely with geocentric distance, to maintain a constant physical aperture size. The initially brightest fragment, *F1*, had a magnitude of $r \sim gri \sim 20$, and the faintest fragment *F9* had $gri \sim 25$.

Figure 2 shows the absolute photometry $m(1, 1, 0)$ obtained by adjusting calibrated magnitude *m* to geocentric and heliocentric distances $\Delta = r_h = 1$ AU and to phase angle $\alpha = 0^\circ$, with the cometary dust phase coefficient $\beta = 0.02$ derived from Meech & Jewitt (1987) and Krasnopolsky et al. (1987).

$$m(1, 1, 0) = m - 5 \log_{10}(r_h \Delta) - 0.02 \times \alpha \quad (2)$$

The uncertainties shown by the error bars are computed from the scatter of measurements taken during one night.

It is immediately evident that the brightest fragment *F1* is growing fainter as it approaches perihelion, a trend that is followed by *F2*, *F3*, and faint fragment *F7*. However, fragment *F4* appears to rise in brightness in the initial *r*-band measurements, and *F5* and *F6* are growing steadily brighter, suggesting that the cloud is evolving rapidly. Most notably, by 30 January, *F4* has increased in brightness by two magnitudes, and is clearly the brightest object. On 31 January, its $m(1, 0, 0) \approx 17.5$ is only about one magnitude fainter than the fading value after the 2010 outburst (Ishiguro et al. 2014, Table 2).

In addition to the data in Fig. 2, we performed photometry on the 4 December PS1 images. We measured both fragment *F1* and the diffuse assemblage at *F2* to have identical magnitudes $r = 21.9 \pm 0.2$ and $m(1, 1, 0)_{gri} = 17.7 \pm 0.2$. For *F1* this magnitude is consistent with the dimming trend seen in the subsequent CFHT observations. For *F2*, this value is roughly consistent with the summed flux of *F2*, *F3*, *F5*, *F6* in the CFHT observations suggesting little evolution in *F1* or *F2*, *F3*, *F5*, *F6* from 4 Dec. The surprising result was the complete absence of concentrated fragment *F4* in the PS1 4 December image. The absence of *F4* may be consistent with the ongoing brightening as seen in Fig. 2, but may also arise from the limitations of the PS1 data.

In a supplementary table to this paper, we present astrometry and photometry of all the fragments in Fig. 2.

4. NON-GRAVITATIONAL FORCES FROM ASTROMETRY

Using our astrometry, we investigated non-gravitational forces acting on on P/2010 V1. We obtained astrometric data from the 2010-2011 apparition from the Minor Planet Center. For the ongoing 2016 apparition, we combined our own CFHT measurements with observations published by the Minor Planet Center through 5 February 2016. Through a series of dust motion simulations, we determined that component *F4* (called P/2010 V1-c by the Minor Planet Center) is the primary nucleus of the comet, because it is the easternmost large fragment. This conclusion is supported by the brightening observed in the later photometry.

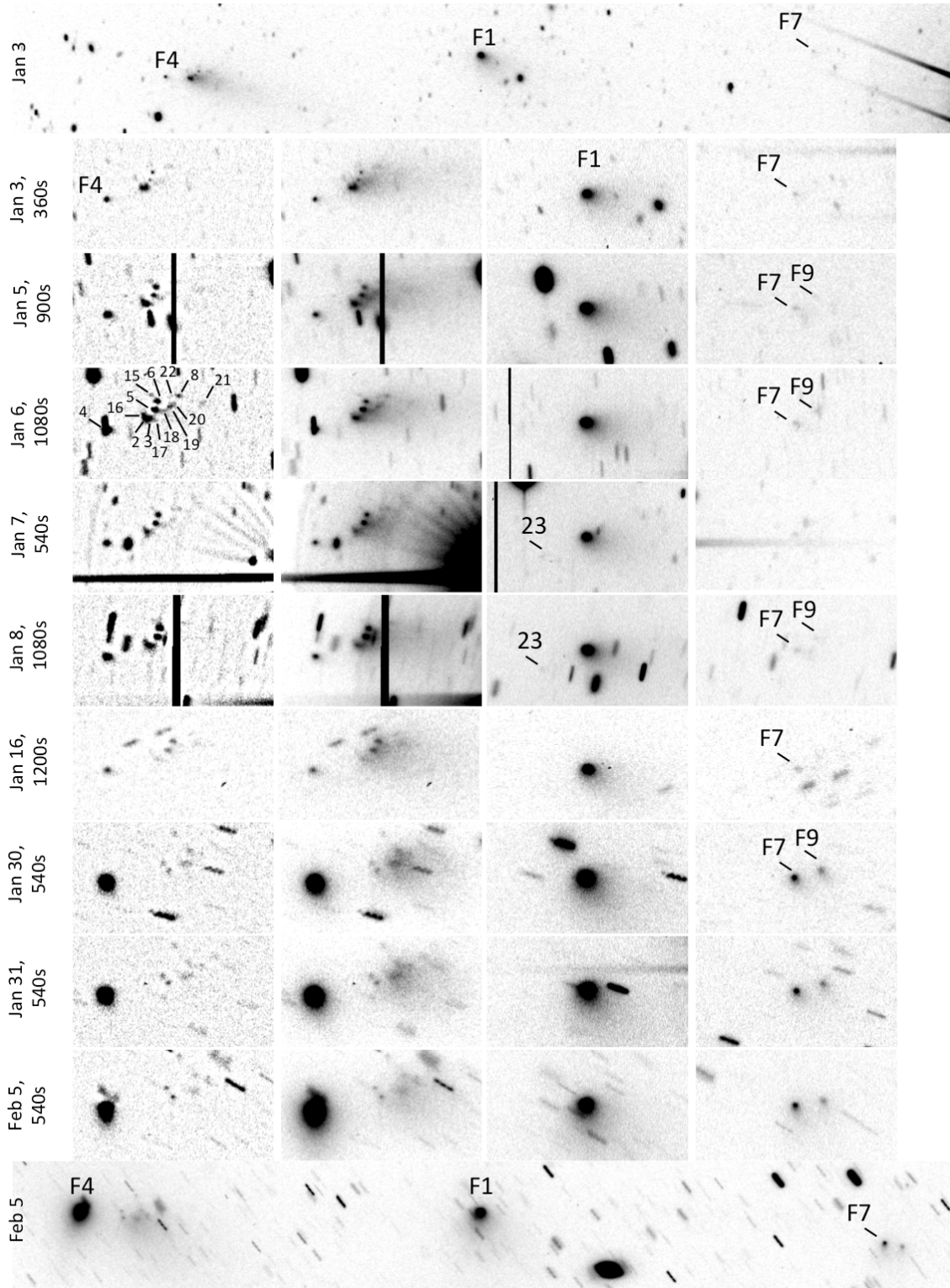


Figure 1. Montage of images of P/2010 V1 from 2016 January 3 to February 5. The top and bottom strips show a portion of the full image rotated by 21° . Each other (multi-pane) row shows $45'' \times 25''$ regions centered on fragments *F4*, *F1*, and *F7*; N is up and E is to the left. The left column is an enhanced (unsharp mask) view of *F4* to show the fragments.

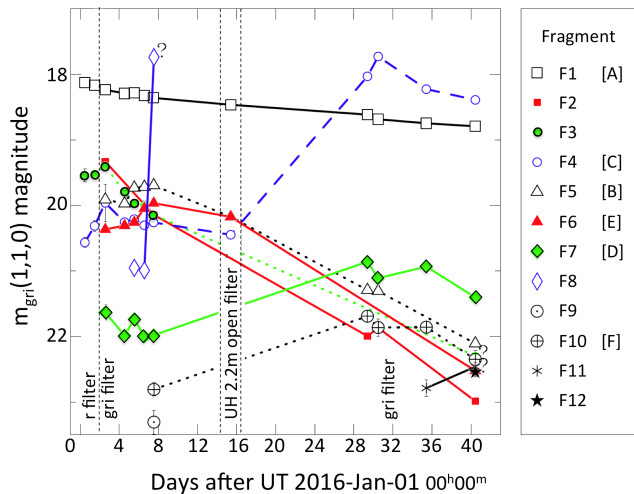


Figure 2. Fragment photometry, magnitudes $m(1,1,0)$, with a question mark indicating a data point based on a single measurement and near a bright star diffraction spike. r magnitudes of first two nights are converted to gri . With a few exceptions, the error bars are smaller than the graph symbols. The letters in the square brackets in the legend indicate the current IAU designations of the fragments; for example, our $F1$ corresponds to P/2010 V1-A.

We employed EXORB² to determine an orbit by linking observations of component $F4$ with nucleus observations from the 2010-2011 apparition. The weights assigned to the observations are based on the scheme described in Chesley et al. (2010) and Farnocchia et al. (2015). The code utilizes the JPL DE431 ephemeris, and includes perturbations from the eight major planets, Pluto, Ceres, Pallas, and Vesta. The code also takes the relativistic effect into consideration, although the contribution is trivial. We applied the symmetric non-gravitational force model of Marsden et al. (1973). The free parameters to be solved were the six orbital elements along with the radial and transverse non-gravitational parameters, A_1 and A_2 .

We found it necessary to exclude two apparently erroneous 2014 observations, because they resulted in $\sim 0.5^\circ$ residuals. Additionally, astrometry with residuals in right ascension and in declination greater than $2''$ was ignored. This threshold was chosen as a compromise between removing outliers and preserving valid observations, and left us with 507 out of 581 initial astrometric measurements.

The best-fit orbital solution gives non-gravitational terms $A_1 = (-5.89 \pm 5.37) \times 10^{-9}$ AU day⁻², and $A_2 = (+7.87 \pm 2.59) \times 10^{-9}$ AU day⁻², with rms = 0.64''. We note that the negative value A_1 is physically meaningless, but is also statistically consistent with zero.

To avoid potential biases and prevent unrealistic weights from being assigned to a subset of observations, we used the Monte Carlo stochastic exclusion function of the code to iterate the orbital solution process 500 times. We then calculated mean values and standard deviations of A_1 and A_2 from the set of realized orbital solutions, and obtained Monte-Carlo values and errors $A_1 = (-5.97 \pm 4.76) \times 10^{-9}$ AU day⁻², and $A_2 = (+7.93 \pm 2.26) \times 10^{-9}$ AU day⁻², consistent with the first run.

Based on the two slightly different methods, we con-

² <http://www.solexorb.it/Solex120/Download.html>

clude that we have no detection in A_1 . However, our finding of a non-zero value for A_2 is a statistically meaningful $\sim 3\sigma$ detection of a positive non-gravitational force, consistent with prograde rotation (Yeomans et al. 2004).

For other fragments, we made no attempt to measure non-gravitational effects from the astrometry because they are the products of a unknown series of fragmentation events.

5. FRAGMENT DYNAMICS

To understand the dynamical properties of the fragments, we make use of the Monte Carlo model developed in our earlier works (e.g. Ye & Hui 2014; Ye et al. 2015, 2016). In detail, our approach creates an ensemble of fragment ejection directions, velocities, and times, and finds those emission events that best match the final observations. Intervals of ejection times that produce more viable matches with the data are deemed more likely than intervals that produce fewer matches.

The continuing fragmentation of the comet makes it challenging to follow each fragment over an extended period of time, especially for fragments in the debris field surrounding fragment $F3$. Hence, we focus on four distinct fragments $F1$, $F3$, $F4$ and $F7$ only. Component $F4$ is the likely primary as discussed; fragments $F1$ and $F7$ are either very bright or distant from the remainder, allowing robust night-to-night associations; fragment $F3$ began as the brightest fragment in the debris field that was unambiguously followed for the longest time span (2016 Jan. 1 to 8), making it a good representative of the debris field as a whole³.

Unarguably, all fragments are the descendants from the primary component $F4$. The question is whether all fragments are the *direct* descendants of $F4$. It is plausible that the fragments continue to split into smaller fragments as already been hinted by the $F2$ - $F3$ debris field. For a given fragment, any fragment to its east could be its direct parent, i.e. $F7$ could be the direct descendant of either $F1$, $F3$ or $F4$, and $F1$ could be directly from either $F3$ or $F4$. However, both $F1$ and $F7$ are apparently “healthy” fragments while $F3$ and its immediate companions are only visible intermittently, we feel it is unlikely for $F3$ (or its direct progenitor) to be the parent of either $F1$ or $F7$. Hence, we explore these two scenarios:

1. $F4$ as the parent of $F1$, $F3$ and $F7$; and
2. $F4$ as the parent of $F1$ and $F3$, while $F1$ as the parent of $F7$.

A total of ~ 20 million hypothetical fragments are released in 10-day steps from the 2010 outburst (circa. 2010 Nov. 1) to the recovery in 2016 (circa. 2016 Jan. 1), from the parent component (either $F1$ or $F4$). The fragments are ejected isotropically at random speeds between 0 and 1 m s⁻¹, a range determined by Sekanina (1982). The dynamics of the fragments are then mainly determined by solar gravity as well as the net radial force due to anisotropic outgassing of the respective fragment, described by the ratio between the force and solar gravity,

³ Fragment $F2$'s astrometry after mid-January 2016 is very poor due to its extremely diffuse appearance, therefore we feel that it is not suitable as the representative fragment.

γ (c.f. Sekanina 1977). We then integrate the fragments to the epoch of 2016 Jan. 8.0 TT using the 15th order RADAU integrator embedded the MERCURY6 package (Everhart 1985; Chambers 1999), accounting for the gravitational perturbations from the eight major planets (including the Earth-Moon barycenter), and radiation pressure. At the end, we compare the modeled *relative* positions between the primary and the fragment with the observations, and record the solutions when the observed minus calculated ($O - C$) error is less than $0.5''$ (roughly half of the FWHM). Henceforth, we refer this set of solutions as “good” solutions.

The demographics of the “good” solutions are shown in Figures 3 and 4. Fragment direction is expressed in the comet’s reference frame, with the Z axis pointing toward the sun, the orthogonal X axis aligned in the negative orbit direction, and the Y axis pointing north from the XZ orbital plane. A fragment’s ejection direction is specified by standard spherical longitude φ and latitude ϑ . That is, $x = \sin \vartheta \cos \varphi$, $y = \sin \vartheta \sin \varphi$, and $z = \cos \vartheta$. Then $\vartheta = 0^\circ$ points at the sun, $\varphi = 0^\circ$ points in the negative sense of orbital motion, and $\varphi = 90^\circ$ points north.

We immediately note that the solutions do not congregate around or shortly after the 2010 outburst, but instead mostly scatter along the comet’s outbound journey. This indicates that the surviving fragments are not immediately produced by the 2010 outburst. For each fragment:

1. The fragmentation of $F1$ from the main nucleus most likely occurred around late 2012 to early 2013, with an uncertainty of about a year. The median solution is $\vartheta = 130^\circ$, $\varphi = 120^\circ$, split speed $0.3 \pm 0.1 \text{ m s}^{-1}$, and $\gamma \sim 2 \times 10^{-5}$, representing an emission in the northern hemisphere at the night-side.
2. The split of fragment $F3$ is complicated by the fact that $F3$ is observationally less constrained. However, we note that most good solutions congregate over recent epochs, within a few months from the recovery in 2015-2016, consistent with the fact that fragment $F3$ is much closer to the primary than fragment $F1$. This, in turn, implies that the split between $F3$ and the primary occur much later than the split between $F1$ and the primary. The good solutions are very scattered across the parameter spaces, but do seem to congregate in the nucleus’ southern hemisphere at the night-side (i.e. $180^\circ < \varphi < 360^\circ$, $90^\circ < \vartheta < 180^\circ$).
3. The simulation favors $F1$ as the direct parent of fragment $F7$, as opposed to $F4$, where only two good solutions are found out of the 20 million trials. The split epoch is hard to tell, but the solutions are congregate around late 2012. However, if $F1$ is the direct parent of $F7$, then the fragmentation must happen after $F1$ split off from $F4$. The demographics of the good solutions look strikingly similar to the good solutions of fragment $F3$ (apart from difference in the timing). If the split between $F1$ and $F7$ did occur some time after late 2012 to early 2013, then the meaningful good solutions are in the twilight zone of the southern hemisphere, with

either a large split speed (at the order of 0.5 m s^{-1}) or a large γ ($\sim 10^{-4}$).

In general, our solution agrees with the general conclusion by Sekanina (2016b,c), that all the surviving fragments are likely not immediately produced by the 2010 outburst. Further refinement of split parameters is challenging, as the determination is highly sensitive to the quality of the astrometry. This is especially true for the sub-fragments in the debris field, where cross-identification between observations from different night/observatory needs to be done with great care.

6. DISCUSSION

It is peculiar that fragment $F1$ was initially brighter than the nucleus $F4$. However, as noted by Sekanina (1982, 2009), split comet fragment size is often unrelated to dust flux.

The previous far larger outburst of comet 17P/Holmes also produced fragments, but these were seen immediately after the event (Stevenson et al. 2010), in contrast to the 2010 outburst of P/2010 V1. In both events, a proposed mechanism for the outburst was the runaway exothermic conversion of CO-laden amorphous ice to the crystalline form, triggered by a perihelion heat wave from the surface (Sekanina 2009; Ishiguro et al. 2014). It is possible that the delay in fragment emission from the initial outburst is the result of a smoldering ongoing crystallization process initiated by the 2010 perihelion. Fig. 1 of Sekanina (2009) shows that the crystallization process has a many-year slow-growth phase before accelerating catastrophically, in agreement with the delayed fragmentation we observe. If such a process hit pockets of CO rich ice, or if it propagated into deep reservoirs where it reached a critical temperature of $\sim 130 \text{ K}$ months or years later, it could create a sequence of delayed post-perihelion splitting events.

In contrast to amorphous ice crystallization, the direct sublimation of CO or other volatiles, even if they survived at the heliocentric distance of P/2010 A2, would be a self-quenching endothermic process.

7. CONCLUSIONS

We performed photometric analysis and dynamical simulations of the fragmented comet P/2010 V1. We found that both dynamical arguments and a strong brightening indicate that $F4$ corresponds to the parent nucleus, which is within a magnitude of the $m(1, 1, 0)$ of the fading post-outburst nucleus in 2011.

Dynamical simulations indicate that the breakup occurred over a period of years after the 2010 October outburst, with eastern fragments $F1$ and $F7$ breaking off as early as 2011.

We thank Simon Prunet for the transformation from g, r, i to the MegaCam gri filter. Q.-Z. thanks Peter Brown for support and Paul Wiegert for computational resources. We thank Dina Prialnik for useful discussions of the physics of activity, and R. Weryk and E. Schunova for UH2.2m observations. Part of the numerical simulations were conducted using the facilities of the Shared Hierarchical Academic Research Computing Network (SHARCNET:www.sharcnet.ca) and Compute/Calcul Canada. M.-T. thanks Aldo Vitagliano

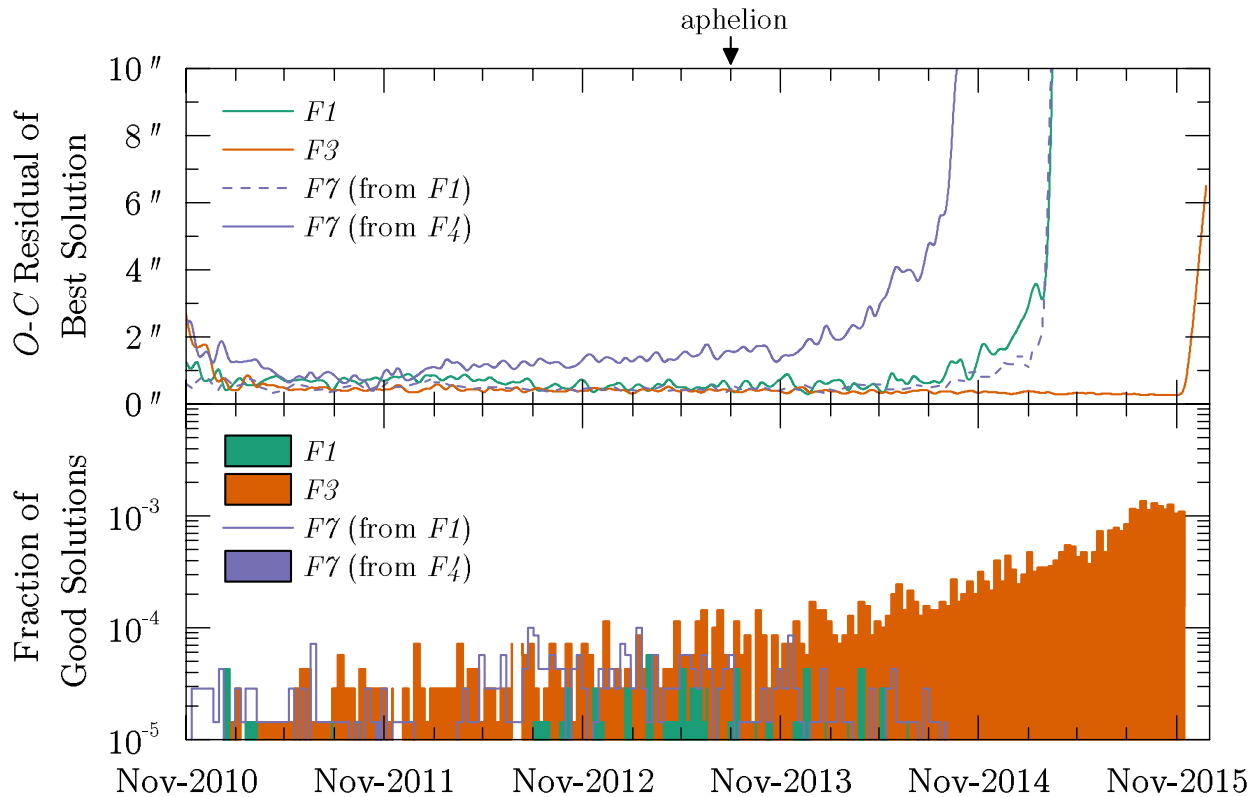


Figure 3. Upper panel: best solutions (i.e. solutions with smallest $O - C$ residuals) at different split epochs; bottom panel: fraction of “good” solutions (i.e. solutions with $O - C$ residual less than half FWHM or $0.5''$). Only those regions of the bottom panel that produce the largest fraction of good detections represent viable ejection times. For example, $F1$ (green) could only have been ejected in a few events around the start of 2011, or many more events between 2012 August and 2013 August.

for an improved version of EXORB. RJW acknowledges support by NASA under grants NNX12AR65G and NNX14AM74G. KJM, JK and JVK acknowledge support through the NASA Astrobiology Institute under Cooperative Agreement NNA08DA77A, and partial support through an award from the National Science Foundation AST1413736. Observations were obtained with MegaPrime/MegaCam, a joint project of CFHT and CEA/DAPNIA, at the Canada-France-Hawaii Telescope (CFHT).

Facilities: CFHT (MegaCam), Pan-STARRS1, UH 2.2m

REFERENCES

- Aihara, H., Allende Prieto, C., An, D., et al. 2011, *ApJS*, 193, 29
 Belton, M. J. S. 2015, *Icarus*, 245, 87
 Bertin, E., Mellier, Y., Radovich, M., et al. 2002, in *Astronomical Society of the Pacific Conference Series*, Vol. 281, *Astronomical Data Analysis Software and Systems XI*, ed. D. A. Bohlender, D. Durand, & T. H. Handley, 228
 Boehnhardt, H. 2004, in *Comets II*, ed. M. C. Festou, H. U. Keller, & H. A. Weaver (University of Arizona Press), 301–316
 Chambers, J. E. 1999, *MNRAS*, 304, 793
 Chesley, S. R., Baer, J., & Monet, D. G. 2010, *Icarus*, 210, 158
 Dekelver, P. J., & Cuppens, W. 2016, *Central Bureau Electronic Telegrams*, 4250
 Everhart, E. 1985, in *Dynamics of Comets: Their Origin and Evolution*, *Proceedings of IAU Colloq. 83*, held in Rome, Italy, June 11–15, 1984. Edited by Andrea Carusi and Giovanni B. Valsecchi. Dordrecht: Reidel, *Astrophysics and Space Science Library*. Volume 115, 1985, p.185, ed. A. Carusi & G. B. Valsecchi, 185
 Farnocchia, D., Chesley, S. R., Chamberlin, A. B., & Tholen, D. J. 2015, *Icarus*, 245, 94
 Ishiguro, M., Jewitt, D., Hanayama, H., et al. 2014, *ApJ*, 787, 55
 Kaiser, N., Aussel, H., Burke, B. E., et al. 2002, in *Proc. SPIE*, Vol. 4836, *Survey and Other Telescope Technologies and Discoveries*, ed. J. A. Tyson & S. Wolff, 154–164
 Krasnopolsky, V. A., Moroz, V. I., Krysko, A. A., Tkachuk, A. Y., & Moreels, G. 1987, *A&A*, 187, 707
 Marsden, B. G., Sekanina, Z., & Yeomans, D. K. 1973, *AJ*, 78, 211
 Meech, K. J., & Jewitt, D. C. 1987, *A&A*, 187, 585
 Sekanina, Z. 1977, *Icarus*, 30, 574
 Sekanina, Z. 1982, in *IAU Colloq. 61: Comet Discoveries, Statistics, and Observational Selection*, ed. L. L. Wilkening, 251–287
 —. 2009, *International Comet Quarterly*, 31, 99
 —. 2016a, *Central Bureau Electronic Telegrams*, 4235
 —. 2016b, *Central Bureau Electronic Telegrams*, 4250
 —. 2016c, *Central Bureau Electronic Telegrams*, 4254
 Sekanina, Z., Chodas, P. W., & Yeomans, D. K. 1994, *A&A*, 289, 607
 Stevenson, R., Kleyna, J., & Jewitt, D. 2010, *AJ*, 139, 2230
 Weryk, R., Wainscoat, R.-J., & Micheli, M. 2016, *Central Bureau Electronic Telegrams*, 4230
 Ye, Q.-Z., Brown, P. G., Bell, C., et al. 2015, *ApJ*, 814, 79
 Ye, Q.-Z., & Hui, M.-T. 2014, *ApJ*, 787, 115
 Ye, Q.-Z., Hui, M.-T., Brown, P. G., et al. 2016, *Icarus*, 264, 48
 Yeomans, D. K., Chodas, P. W., Sitarski, G., Szutowicz, S., & Królikowska, M. 2004, in *Comets II*, ed. M. C. Festou, H. U. Keller, & H. A. Weaver (University of Arizona Press), 137–151

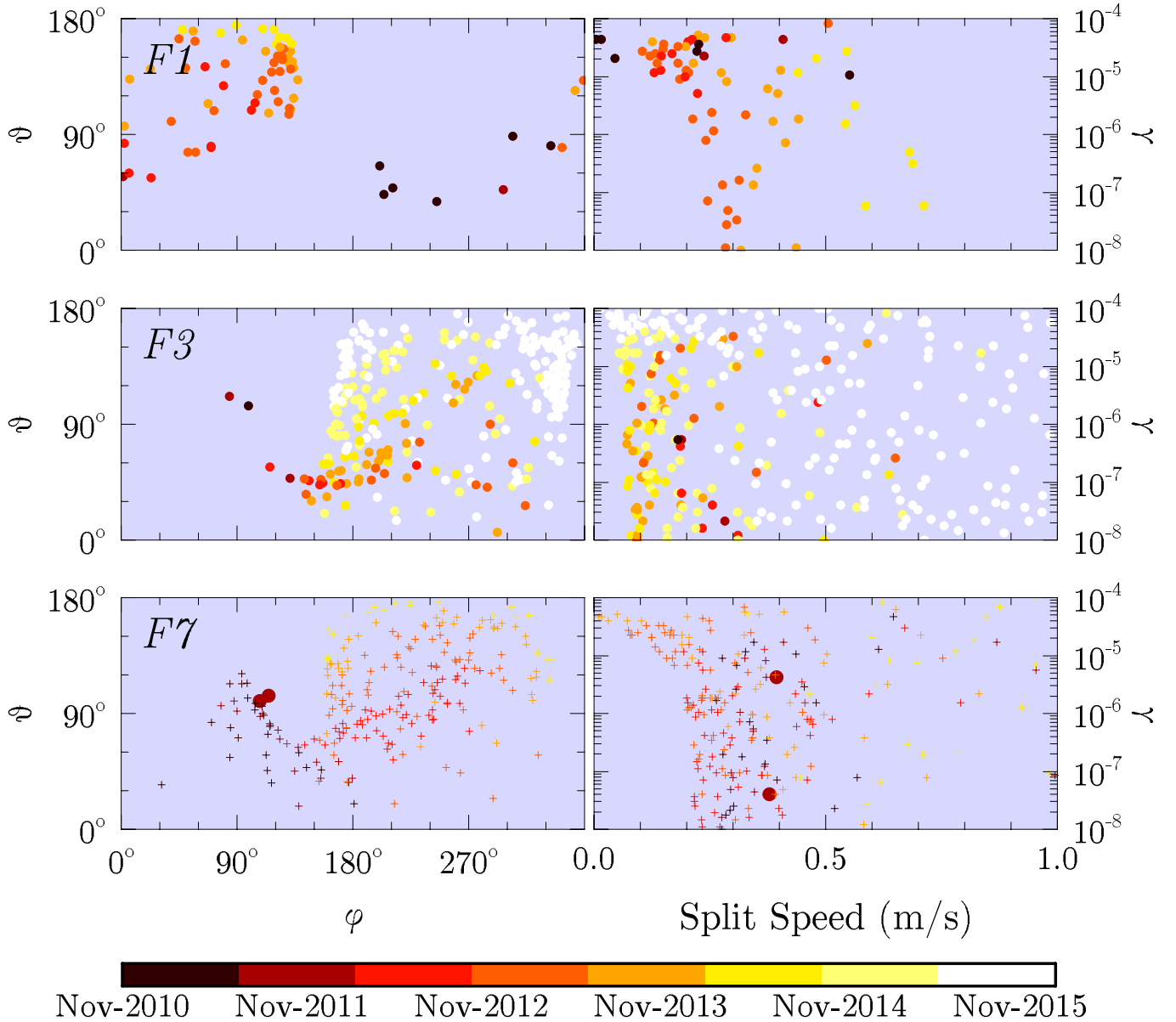


Figure 4. Split direction (left column) as well as split speed and deceleration parameter γ (right column) for good solutions ($O - C$ residuals less than $0.5''$) for fragments $F1$ (upper row), $F2$ (middle row) and $F7$ (bottom row). The data points for fragment $F2$ are under-sampled for clarity. Color denotes different split epoch, filled circle denotes to the scenario that fragment $F4$ is the parent and cross denotes to the scenario that fragment $F1$ is the parent. φ and ϑ are the longitude and latitude in a standard spherical coordinate system, with the Z axis pointing toward the sun, the orthogonal X axis aligned in the negative orbit direction, and the Y axis pointing north from the XZ orbital plane. γ is the ratio of anisotropic outgassing force of the respective fragment to the solar gravity.